

PRELIMINARY REPORT ON THE RESULTS OF ROCKET EXPERIMENTS AT SYOWA STATION IN 1984

Takesi NAGATA, Takeo HIRASAWA, Masaki EJIRI and Takayuki ONO

National Institute of Polar Research, 9-10, Kaga 1-chome, Itabashi-ku, Tokyo 173

Abstract: Results of the experiments with the sounding rockets at Syowa Station, Antarctica, are presented preliminarily. Three rockets penetrated into the bright active arc (~ 8 kR for 4278 \AA) during the breakup phase, the quiet stable arc (~ 3 kR) during the pre-breakup phase and the diffuse auroras ($2\sim 3$ kR) during the post-breakup phase of auroral substorms.

The peak of electron density amounts to $2 \times 10^5 \text{ ele/cm}^3$ at 120 km in altitude, $2 \times 10^5 \text{ ele/cm}^3$ at 100 km and $6 \times 10^4 \text{ ele/cm}^3$ at 150 km for bright active, the quiet stable and the diffuse auroras, respectively, while the diffuse aurora has the secondary peak of electron density with the amount of $2 \times 10^4 \text{ ele/cm}^3$ at 100 km in altitude. The vertical profiles of auroral $\lambda 4278 \text{ \AA}$ emissions for the three auroras of different types show that the height of maximum $\lambda 4278 \text{ \AA}$ emission is in agreement with the height (120 km) of the peak layer of electron density in the breakup active auroras and in agreement with the height (95~100 km) of the secondary peak layer of electron density in the post-breakup diffuse auroras. The energy spectra of precipitating electrons measured by three rockets suggest that the auroral arcs are excited mostly by the auroral electrons of 1~5 keV in energy.

1. Introduction

In April–May of 1984, three sounding rockets of S-310JA type were launched from Syowa Station (geomagnetic latitude= 69.6°S , geomagnetic longitude= 79.4°) for measuring the electron density and temperature of the ionosphere, auroral patterns and luminosity *in situ* and the energy spectra of auroral particles in the pre-breakup, breakup and post-breakup phases of auroral substorms.

The maximum altitude and direction of rocket orbits are 202~209 km and $308^\circ \sim 310^\circ$, respectively, where the geomagnetic north at Syowa Station is 314° . The launching time, the maximum altitude, the horizontal distance and the flight period for the three rocket flights are listed in Table 1.

Table 1. Table of the rocket launching at Syowa Station in April–May 1984.

	S-310JA-8	S-310JA-9	S-310JA-10
Launching time (UT)	1927: 01	2214: 10	2317: 13
	April 4, 1984	May 3, 1984	May 28, 1984
Maximum altitude (km)	201.8	204.0	208.8
Horizontal distance (km)	227.5	223.1	220.0
Flight time	7 min 09 s	7 min 17 s	7 min 21 s

2. Auroral Substorms observed on the Ground during Rocket Flight

Figures 1, 2 and 3 show the ground-based data of auroral substorms observed at Syowa Station on the days when the flights of three rockets were carried out. In these figures, the time variations of (a) geomagnetic H -component (ΔH), (b) the intensity of auroral $\lambda 4278 \text{ \AA}$ ($I(\lambda 4278)$) (geomagnetically northward 45° in zenith angle), (c) VLF hiss intensity of 30 kHz band (VLF) and (d) the cosmic noise absorption (CNA) are illustrated from the top to the bottom.

During the flight of S-310JA-8, a sharp negative decrease of -500 nT was observed in the H -component magnetic field variation. Auroral emission ($I(\lambda 4278)$) showed a sharp increase of about 8 kR at peak and CNA amounted to about -0.5 dB , while VLF hiss, which had been observed before the commencement of a sharp magnetic substorm, was suddenly diminished (Fig. 1). Namely, the period of the S-310JA-8 flight was just in coincidence with the breakup phase of a sharp auroral and magnetic substorm.

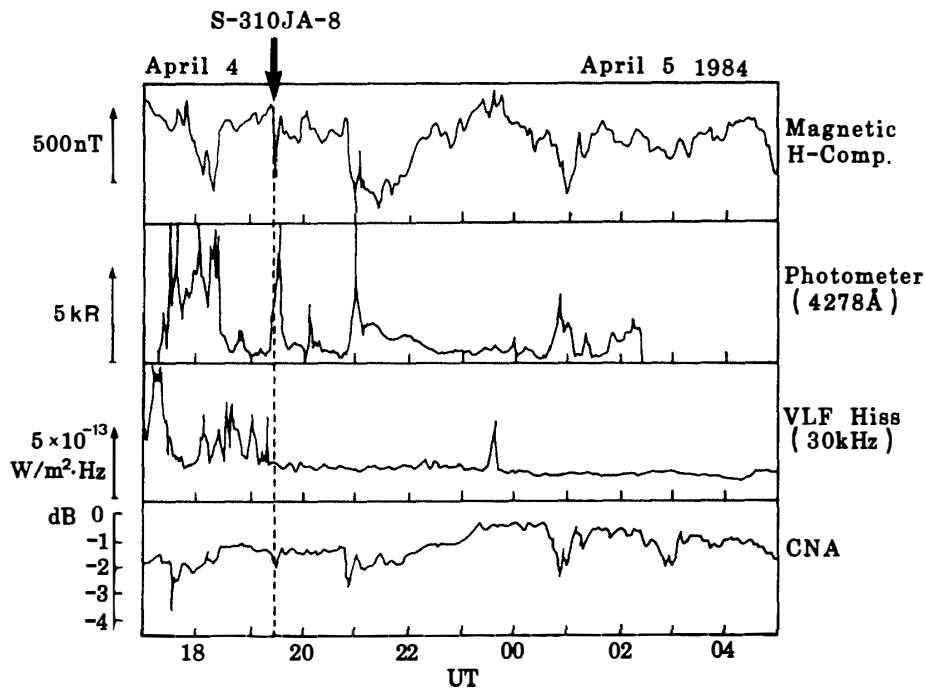


Fig. 1. Ground-based observation data for a breakup stage of a sharp active aurora (April 4, 1984).

During the flight of S-310JA-9, the magnetic field variation (ΔH) was quiet. $I(\lambda 4278)$ was about 3 kR . Any appreciable change was not observed in CNA, while VLF hiss took place for a while before the rocket flight. However, a substorm breakup started about 20 min after the launching of the rocket. The substorm is characterized by $H \simeq -300 \text{ nT}$, $I(\lambda 4278) \simeq 8 \text{ kR}$ and $\text{CNA} \simeq -1 \text{ dB}$ at their maximum stages (Fig. 2). Namely, the flight period of S-310JA-9 corresponded to the pre-breakup phase of an auroral and magnetic substorm.

During the flight of S-310JA-10, $\Delta H = -300 \sim -500 \text{ nT}$, $I(\lambda 4278) = 2 \sim 3 \text{ kR}$ and $\text{CNA} \sim -1.0 \text{ dB}$ (Fig. 3). As shown in Fig. 3, the flight period of S-310JA-10

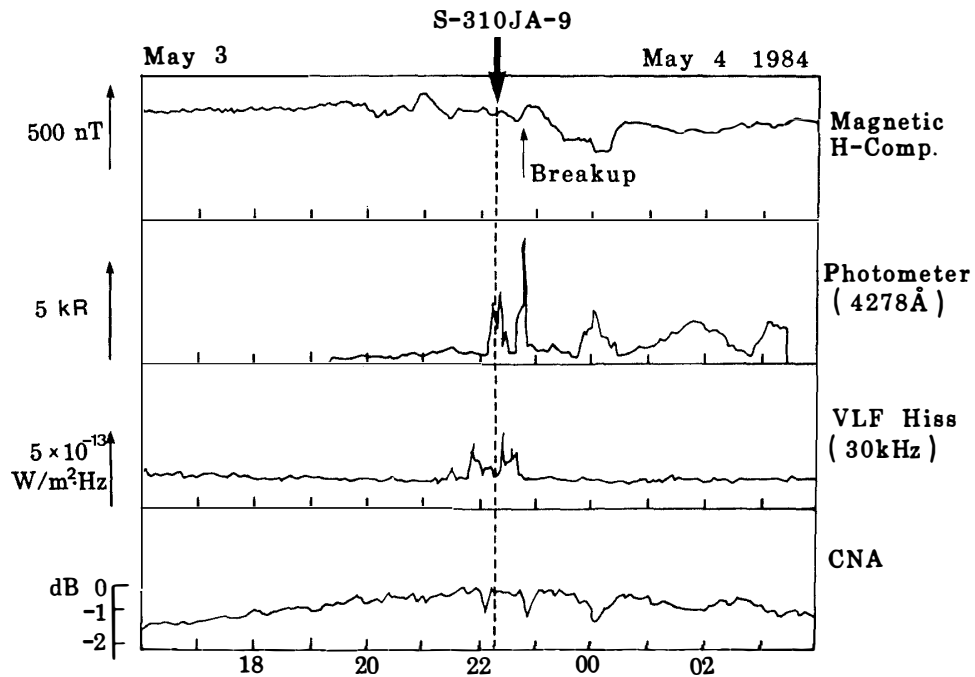


Fig. 2. Ground-based observation data for a pre-breakup stage of auroral activity, when stable auroral arcs were taking place (May 3, 1984).

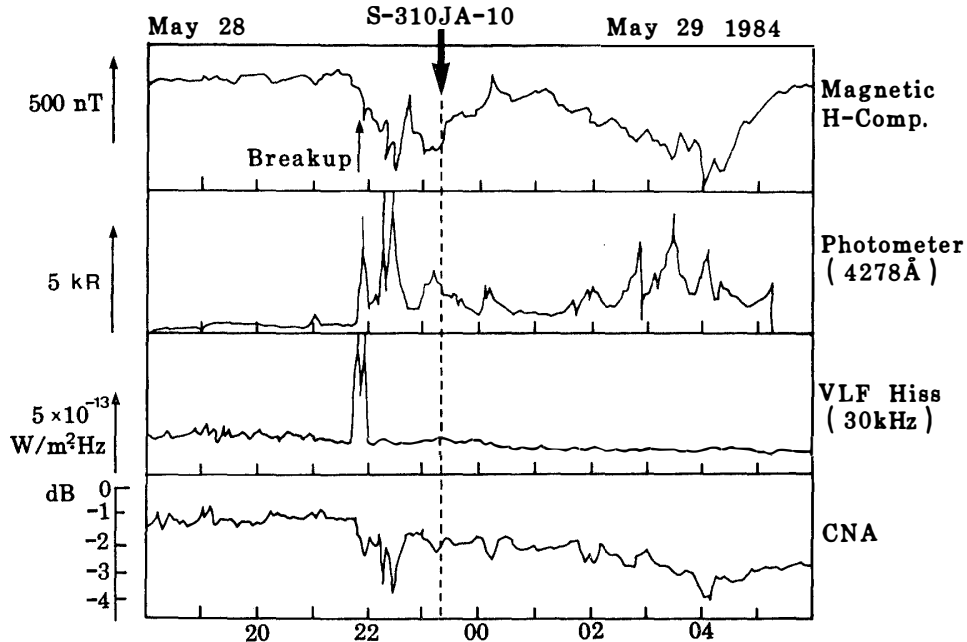


Fig. 3. Ground-based observation data for a post-breakup stage of auroral activity, when diffuse auroras were being displayed over the zenith area (May 28, 1984).

corresponded to the post-breakup phase of an auroral and magnetic substorm. The main phase of the substorm is characterized by $H \simeq -700$ nT and $I(4278) \simeq 7.5$ kR.

In reference to the simultaneous ground-based data obtained by the all sky auroral camera and an auroral scanning photometer, the types of auroras during the flight

periods of three rockets can be signified as breakup active aurora for S-310JA-8, pre-breakup evening-side auroral arc for S-310JA-9 and post-breakup diffuse aurora for S-310JA-10 (*cf.* HIRASAWA and NAGATA, 1972).

3. Electron Number Density Profile

Figure 4 shows the vertical profiles of electron number density in the cases of three auroral activity stages, *i.e.* pre-breakup evening-side auroral arc, breakup active aurora and post-breakup diffuse aurora. In the breakup active aurora, the maximum electron number density $(N_e)_{\max}$ and the height of maximum electron number density

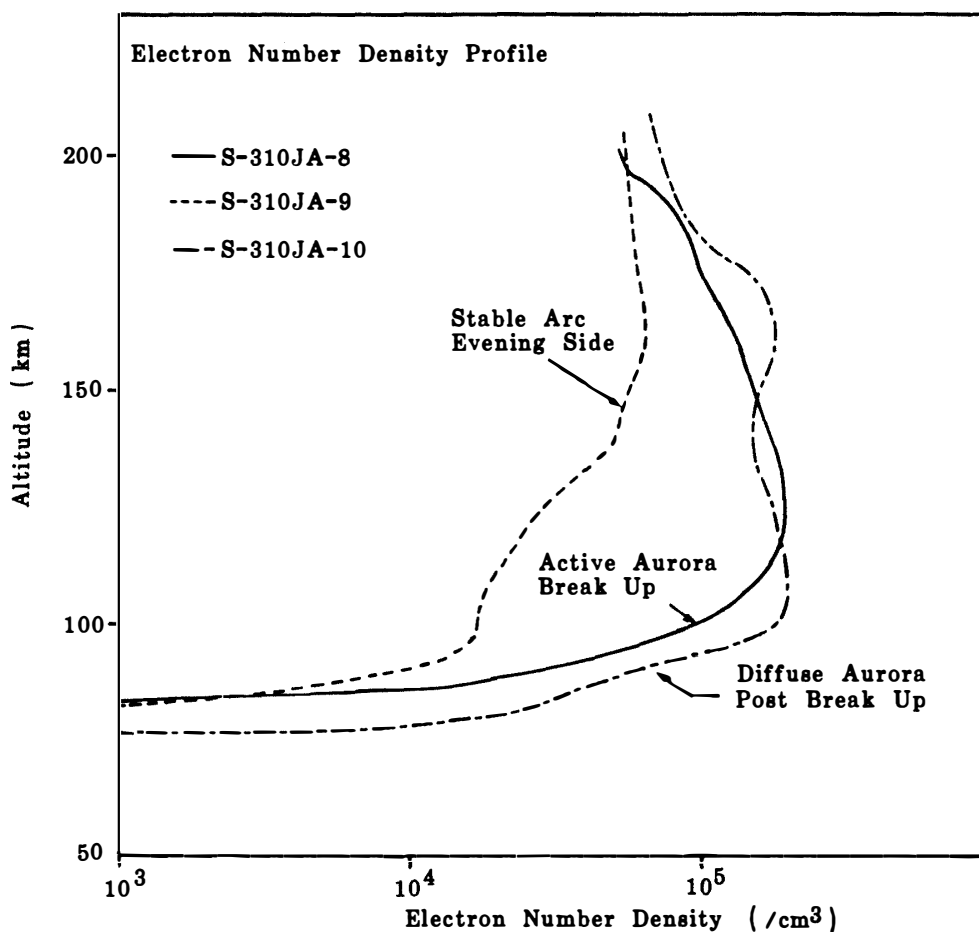


Fig. 4. Vertical profiles of the electron number density in pre-breakup, breakup and post-breakup phases of auroral substorms.

$(h)_{N_e \max}$ are 2×10^5 ele/cm³ and 120 km, respectively. In the post-breakup diffuse aurora, the profile of electron number density has two peaks; namely, $(N_e)_{\max} \simeq 2 \times 10^5$ ele/cm³ and $(h)_{N_e \max} \simeq 100$ km for the major $(N_e)_{\max}$ layer, and $(N_e)_{\max} \simeq 1.5 \times 10^5$ ele/cm³ and $(h)_{N_e \max} \simeq 160$ km for the upper secondary $(N_e)_{\max}$ layer. The bottom of the ionospheric *D*-layer comes down to about 80 km in altitude in the diffuse aurora observed in the post-breakup phase of an auroral substorm. In the pre-

breakup evening-side auroral arc, $(N_e)_{\max}$ is 6×10^4 ele/cm³ at $(h)_{N_e \max} \simeq 150$ km for the major $(N_e)_{\max}$ layer and $(N_e)_{\max}$ is 2×10^4 ele/cm³ at $(h)_{N_e \max} = 95 \sim 100$ km for the lower secondary $(N_e)_{\max}$ layer. The dependence of the electron density profile on the differences of the auroral types is due to the energy spectrum and flux of precipitating auroral electrons and the composition and structure of the ionosphere (REES, 1963; KAMIYAMA, 1966). Hence, the situation can be examined by synthesizing all observed data of the vertical profiles of Ne, auroral emission rate and precipitating auroral particles.

4. Vertical Profile of Auroral Photoemission

The vertical profiles of auroral photoemission are obtained by differentiating the photometric data of auroral 4278 Å emission observed by a downward-looking photometer aboard an ascending rocket. Figure 5 shows the vertical profiles of 4278 Å photoemission for auroras of three different types.

Compared with the vertical profiles of electron density in Fig. 4, the height of maximum $\lambda 4278$ Å emission is in agreement with $(h)_{N_e \max} = 120$ km in the case of the breakup active aurora and is in agreement with $(h)_{N_e \max} \simeq 100$ km for the major (lower) $(N_e)_{\max}$ layer in the post-breakup diffuse aurora. It will be noted, however, that the peak $\lambda 4278$ Å emission rate in the post-breakup diffuse aurora is much smaller than that in the breakup active aurora and that the $\lambda 4278$ Å emission extends upward over

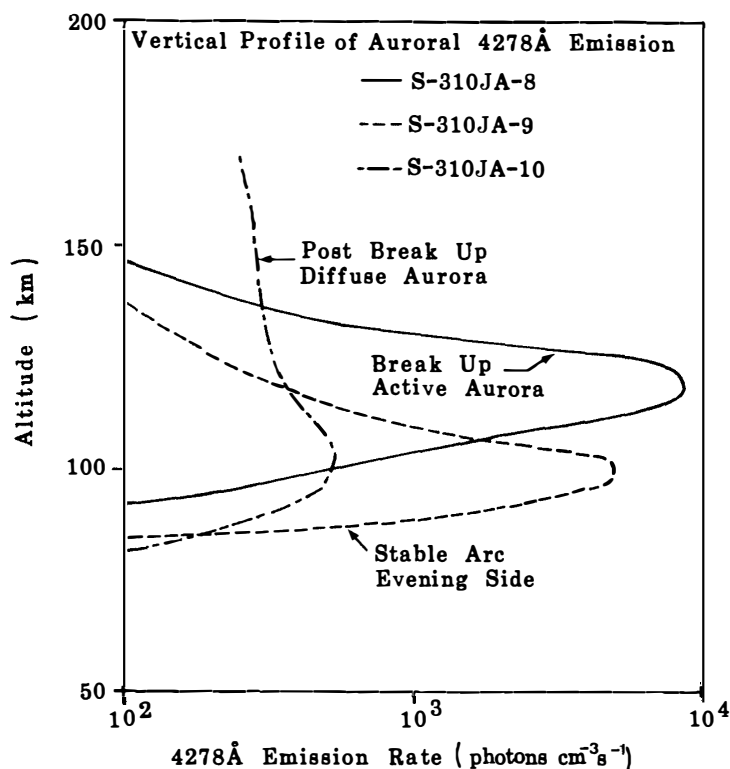


Fig. 5. Vertical profiles of the $\lambda 4278$ Å auroral emission in pre-breakup, breakup and post-breakup phases.

170 km in altitude. In the evening-side auroral arc, the height of the peak $\lambda 4278 \text{ \AA}$ emission layer approximately coincides with $(h)_{N_{e\max}} = 95 \approx 100 \text{ km}$ for the secondary (lower) $(N_e)_{\max}$ layer. No peak of auroral emission corresponding to the major $(N_e)_{\max}$ layer at $(h)_{N_{e\max}} \approx 150 \text{ km}$ is observed.

5. Energy Spectrum of Auroral Electrons

The energy spectra of precipitating electrons were measured every 0.5 s during the flight of the three rockets. For a standard example, the energy spectra of precipitating auroral electrons observed at 170 km in altitude in the ascending orbit for the three auroral activity stages are illustrated in Fig. 6. As shown in the figure, the auroral electron energy spectrum has a peak around 7 keV and the electron flux sharply decreases with increasing electron energy in the energy range beyond 7 keV in the breakup

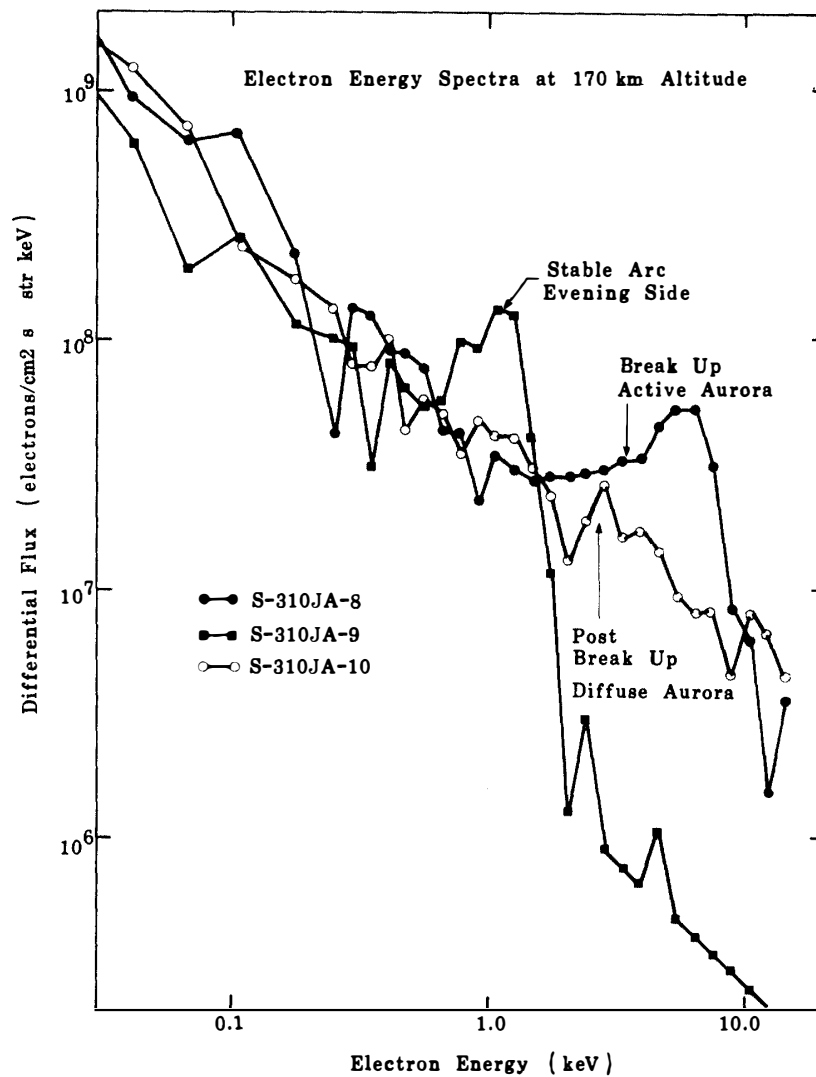


Fig. 6. Energy spectra of precipitating auroral electrons at 170 km altitude in a pre-breakup stable arc.

active aurora, while it has a peak around 1 keV and the electron flux sharply decreases with increasing electron energy in the energy range beyond 1 keV in the pre-breakup evening-side auroral arc. However, the energy spectrum of auroral electron in the post-breakup diffuse aurora shows no distinct peak, but the electron flux monotonously decreases with increasing energy in the observed energy range from 0.1 to 14 keV.

Another topic of the precipitating auroral electron beam is the distribution of electron energy within the cross section of the beam. Rocket S-310JA-9 passed almost horizontally over a stable auroral arc near the apex of the flight orbit (*i.e.* at about 200 km in altitude). Figure 7 shows the energy spectra of auroral electron just on the outside and the inside of the auroral arc. On the inside of the auroral arc, the auroral electron flux is nearly flat for the energy range of 0.5~5 keV with a sharp decrease of the flux beyond 5 keV in energy, while on the outside of the auroral arc, the energy spectrum is nearly flat in the range of 0.2~1.0 keV with a sharp upper cut at about 1 keV. This result suggests that the auroral arc is excited mostly by the auroral electrons of 1~5 keV in energy.

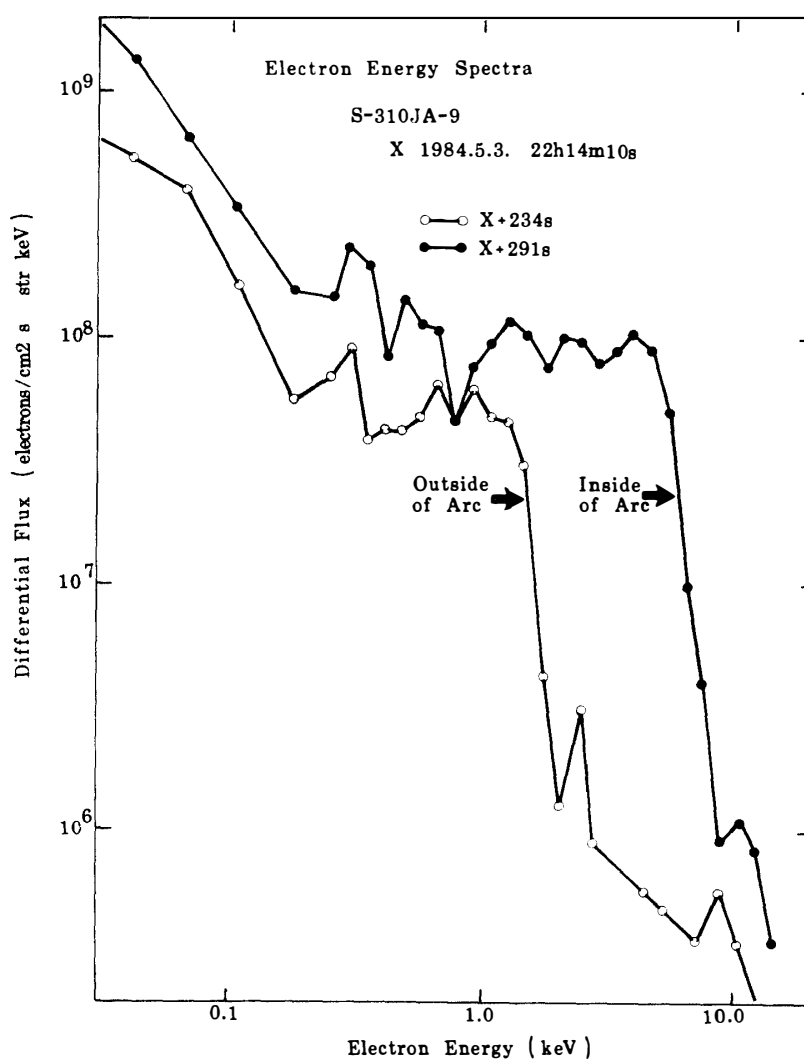


Fig. 7. Energy spectra of precipitating auroral electron inside and outside of a stable arc.

6. Configurations of Auroral Patterns *in situ*

A high sensitive digital auroral TV camera of $30^\circ \times 53^\circ$ in image field area was operated in the downward direction for observing the auroral illuminance distribution *in situ* in each flight of the rocket. The observed auroral illuminance image must be corrected in regard to the image location and the illuminance scale in order to obtain the final precise distribution pattern of auroral illuminance. Figures 8, 9 and 10 illustrate the observed auroral illuminance image at three successively changing heights in each rocket flight, without the necessary corrections. Here, numerals 1, 2, . . . 9, and alphabets A, B, . . . F indicate the auroral illuminance relative scales in the order of $1 < 2 < 3 < 4 < 5 < 6 < 7 < 8 < 9 < A < B < C < D < E < F$. Figure 8 shows successive downward auroral illuminance patterns at 120, 127 and 133 km in altitude observed

Auroral Image Observed by CCD TV Camera

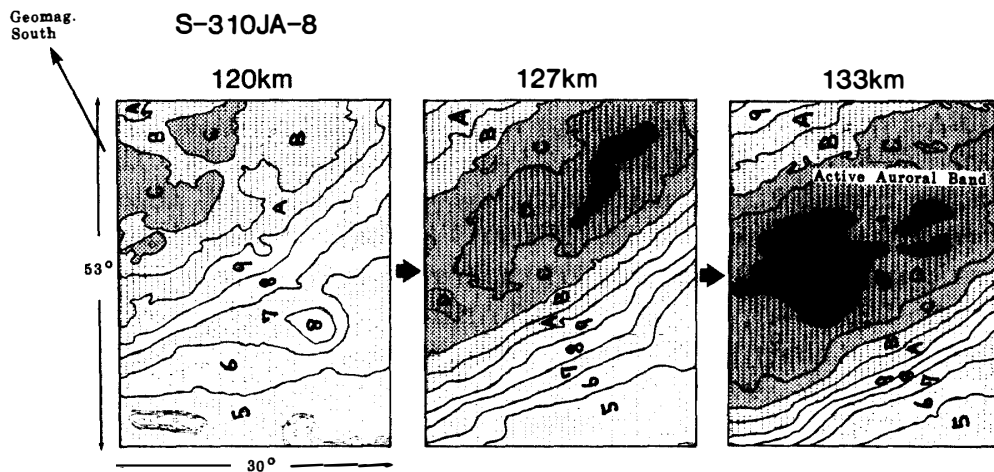


Fig. 8. Successive auroral illuminance images taken downward from a rocket in a breakup stage.

Auroral Image Observed by CCD TV Camera

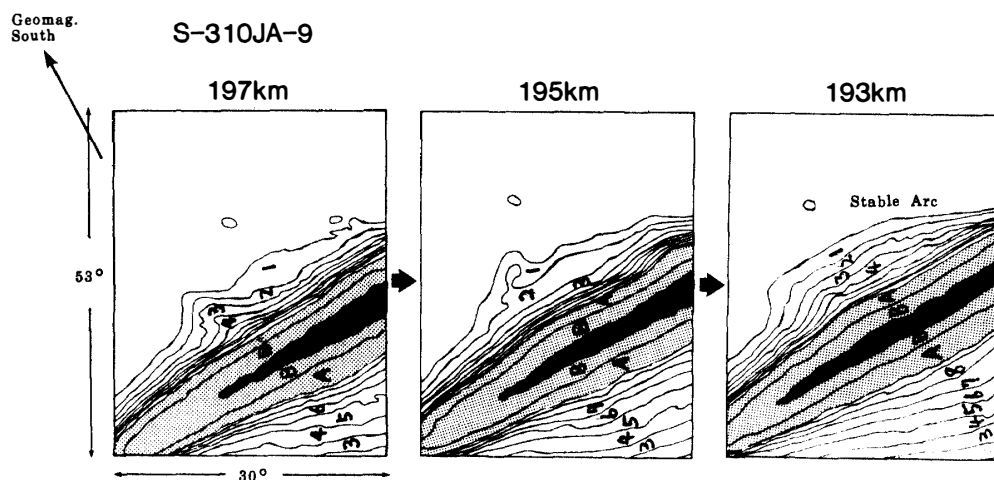


Fig. 9. Successive auroral illuminance image taken downward from a rocket. Stable auroral arc in a pre-breakup stage.

Auroral Image Observed by CCD TV Camera

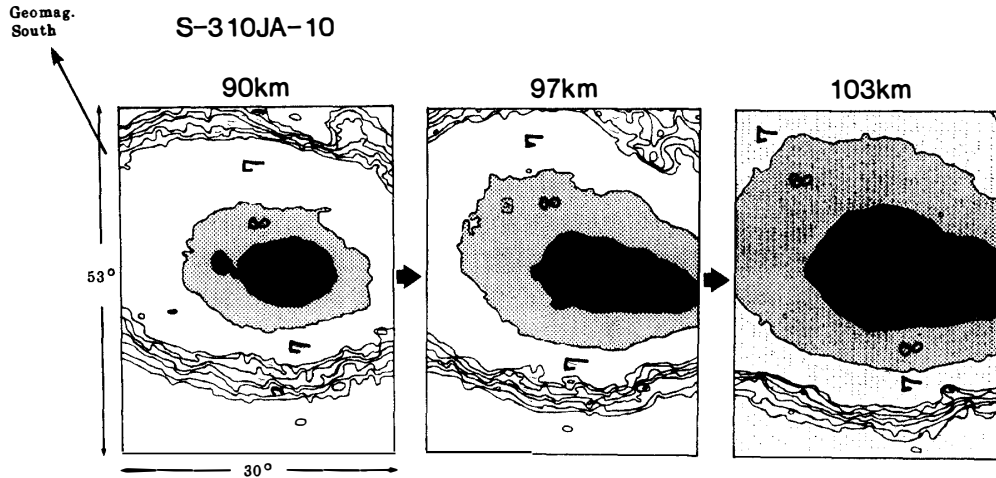


Fig. 10. Successive auroral illuminance image taken downward from a rocket. Diffuse aurora in a post-breakup stage.

by S-310JA-8 during its passing through the $\lambda 4278$ aurora emission layer, where $E \geq 17.8$, $D > 16.0$, $A > 10.6$, $7 > 5.2$ and $5 > 2.1$ mlx in illuminance scale. The illuminance of an active auroral band running along the geomagnetic $E-W$ direction becomes intensified with increasing altitude. Figure 9 shows successive downward auroral illuminance patterns at 197, 195 and 193 km in altitude observed by S-310JA-9, where $C > 18.2$, $A > 5.3$, $7 > 4.3$, $5 > 3.6$ and $3 > 2.9$ mlx. Since the observed stable auroral arc was located at about 100 km in altitude at that time (Fig. 5), the observed auroral illuminance image is very stable in Fig. 9. Figure 10 shows successive downward illuminance patterns at 90, 97 and 103 km in altitude observed by S-310JA-10 during its passing through the lower $\lambda 4278$ emission peak layer of the diffuse aurora (Fig. 5), where $F > 14.8$, $E > 13.0$, $B > 7.9$, $8 > 2.8$ and $7 > 2.1$ mlx. It seems that a relatively intense spot of local aurora took place at altitude lower than even 90 km at that time.

7. Summary

In comparison of Fig. 6 with Figs. 4 and 5, it is qualitatively pointed out that the energy spectrum peak around 7 keV in the breakup active aurora corresponds to $(N_e)_{\max}$ and 4278 \AA aurora emission peak at 120 km in altitude, while the energy spectrum peak around 1 keV in the pre-breakup stable arc corresponds to $(N_e)_{\max}$ around 150 km in altitude. It is also noted that the broad energy spectrum of auroral electron in the post-breakup diffuse aurora explains the vertically large thickness of the ionized layer and the 4278 \AA auroral emission layer. However, in order to illustrate the distinct discrete layer of 4278 \AA auroral emission at about 100 km in altitude in the pre-breakup stable arc and the observed high ionization around 100 km in altitude in the post-breakup diffuse auroras, further detailed examinations are needed. Quantitative discussions on the ionization and excitation processes of the polar atmosphere caused by the precipitating electrons in the different stages of auroral substorm activity will be made by using all observed data of auroral electron energy spectrum.

Figures 8 through 10 are just examples of the top-side photometry of auroras. Analyses in detail of these rocket-borne photographic and photometric data of auroras will be carried out with reference to the simultaneous data of ground-based auroral observations.

References

- HIRASAWA, T. and NAGATA, T. (1972): Constitution of polar substorm and associated phenomena in the southern polar region. *JARE Sci. Rep., Ser. A (Aeronomy)*, **10**, 1-76.
- KAMIYAMA, H. (1966): Ionization and excitation by precipitating electrons. *Rep. Ionos. Space Res. Jpn.*, **20**, 171-187.
- REES, M. H. (1963): Auroral ionization and excitation by incident energetic electrons. *Planet. Space Sci.*, **11**, 1209-1218.

(Received July 10, 1985 ; Revised manuscript received September 24, 1985)